Aircraft observations of boundary layer turbulence: Intermittency and the cascade of energy and passive scalar variance

Citation: Cho, John Y. N. et al. "Aircraft Observations of Boundary Layer Turbulence: Intermittency and the Cascade of Energy and Passive Scalar Variance." Journal of Geophysical Research: Atmospheres 106, D23 (December 2001): 32469–32479 © 2001 American Geophysical Union

As Published: http://dx.doi.org/10.1029/2001JD900079

Publisher: American Geophysical Union (AGU)

Persistent URL: http://hdl.handle.net/1721.1/110979

Version: Final published version: final published article, as it appeared in a journal, conference proceedings, or other formally published context

JOURNAL OF GEOPHYSICAL RESEARCH, VOL. 106, NO. D23, PAGES 32,469–32,479, DECEMBER 16, 2001

Aircraft observations of boundary layer turbulence: Intermittency and the cascade of energy and passive scalar variance

John Y. N. Cho
Department of Earth, Atmospheric, and Planetary Sciences, Massachusetts Institute of Technology, Cambridge, Massachusetts

Bruce E. Anderson, John D. W. Barrick, and K. Lee Thornhill
NASA Langley Research Center, Hampton, Virginia

Abstract. We analyze boundary layer velocity and temperature measurements acquired by aircraft at 22 Hz. The calculated longitudinal velocity third-order structure function yields approximate agreement with Kolmogorov's four-fifths law for the scale range ~10–100 m with a downscale energy flux of $\sim 4 \times 10^{-5}$ m^2 s^{-3}. For scales greater than ~10 km the sign is reversed, implying an inverse energy cascade with an estimated flux of $\sim 10^{-5}$ m^2 s^{-3} associated with two-dimensional stratified turbulence. The mixed structure function of longitudinal velocity and squared temperature increment follows Yaglom's four-thirds law in the same scale range, yielding an estimated downscale temperature variance flux of $\sim 5 \times 10^{-7}$ K^2 s^{-1}. Analysis of higher-order structure functions yields anomalous scaling for both velocity and temperature. The scaling also reveals second-order multifractal phase transitions for both velocity and temperature data. Above the transition moments, asymptotes varying with the number of realizations argue against the log-Poisson model. The log-Lévy model is better able to explain the observed characteristics.

1. Introduction

During NASA's Pacific Exploratory Mission in the Tropics, Phase B (PEM-Tropics B), a turbulent air motion measurement system (TAMMS) with a 22-Hz effective sampling rate was flown on board the P-3B. Although characterization of atmospheric chemistry was the primary raison d'être for the campaign, such high-resolution data are amenable to multiscale analysis of dynamical and scalar advective processes. Encouraged by our recent success in applying structure functions and scaling techniques to mesoscale and large-scale data collected by aircraft in extracting new information about the energy [*Cho and Lindborg*, 2001; *Lindborg and Cho*, 2001] and scalar variance [*Lindborg and Cho*, 2000] cascades, and the intermittency of advected scalars [*Cho et al.*, 2000, 2001], we shift our focus to smaller scales made accessible by the higher sampling rate of TAMMS. At a nominal air speed of 130 m s^{-1} the corresponding spatial resolution is 6 m, which is getting down to the inertial subrange of fully developed turbulence. Thus we have an opportunity to compare the observations with the theories of three-dimensional (3-D) turbulence and to coopt the formalisms already developed for such studies.

Our aim here is to compare observations of tropical marine boundary layer turbulence to theories predicting the second- and third-order structure functions of velocity and temperature as well as the multifractal parameters calculated from higher-order structure functions. We will begin with some relevant background on turbulence theory, move on to the results, then conclude with a summary discussion.

2. Background

In the study of atmospheric turbulence the velocity variance spectrum E has usually been the paradigm of choice for comparisons between theory and observation. This choice has been motivated by the celebrated theoretical inertial subrange spectrum for 3-D isotropic turbulence,

$$E = C_2' \epsilon^{\frac{2}{3}} k^{-\frac{5}{3}} , \tag{1}$$

where C_2' is a constant, ϵ is the mean energy dissipation rate, and k is the wave number. This spectral form follows from universality assumptions and dimensional analysis made by *Kolmogorov* [1941a]. Less often used are the structure functions of velocity defined by

$$S_m = \langle [\delta u(r)]^m \rangle , \tag{2}$$

Paper number 2001JD900079.
0148-0227/01/2001JD900079$09.00

where m is the integer order and the angle brackets denote ensemble averaging. Here $\delta u = u' - u$ is the difference in velocity components between two points $\boldsymbol{x}'$ and $\boldsymbol{x}$ that are separated by distance r. Since the spectral power law lies between k^{-1} and k^{-3} (i.e., a nonstationary signal with stationary increments), the Wiener-Khinchine relation asserts a Fourier duality between E and the second-order structure function such that $S_2 = C_2\epsilon^{2/3}r^{2/3}$, where C_2 is a constant. According to Kolmogorov's universality assumptions C_2 and C_2' ought to be universal constants. This result, however, was questioned by Landau [*Kolmogorov*, 1942], and it has been shown that the third-order structure function relation derived by *Kolmogorov* [1941b] from the Kármán-Howarth equation [*von Kármán and Howarth*, 1938],

$$\left\langle (\delta u_L)^3 \right\rangle = -\frac{4}{5}\epsilon r\,, \tag{3}$$

where u_L is the longitudinal (parallel to r) component of the velocity, is the more fundamental result, derivable from symmetry postulates without universality assumptions [*Frisch*, 1995]. The $-4/5$ value is exact and does not need to be determined empirically. The relation (3) also contains more information than (1) in that the sign of the structure function indicates the direction of the energy cascade [*Frisch*, 1995; *Lindborg*, 1996]: forward (large to small scales) if negative, and reverse (small to large scales) if positive. Relation (3) is actually a special case of a more general energy flux equation

$$\left\langle (\delta u_L)^3 \right\rangle + 2\left\langle \delta u_L\,(\delta u_T)^2 \right\rangle = -\frac{4}{3}\epsilon r\,, \tag{4}$$

where u_T is the transverse (perpendicular to the separation vector $\boldsymbol{x}' - \boldsymbol{x}$) velocity component [*Lindborg*, 1996; *Antonia et al.*, 1997].

Higher-order structure functions yield intermittency information. An absolute-value version of (2), $S_p = \langle |\delta u(r)|^p \rangle$, is often used, where p can be any real number. Then for an interval over r in which scaling prevails in the structure functions, one can determine the exponent ζ_p in

$$S_p \propto r^{\zeta_p}\,. \tag{5}$$

Kolmogorov's [1941] theory (hereafter K41) predicted $\zeta_p = p/3$, which is a special case of monofractal or simple scaling, where ζ_p/p is a constant. If ζ_p/p deviates from a constant value, then the terms multifractal or anomalous scaling are used. Phenomenologically, the amount of departure from simple scaling measures the degree of intermittency in the velocity field. The direction of deviation is such that ζ_q is concave ($d^2\zeta_p/dp^2 < 0$) [*Davis et al.*, 1994].

There is now considerable experimental and numerical evidence that $\zeta_p \neq p/3$ [e.g., *Anselmet et al.*, 1984; *Vincent and Meneguzzi*, 1991]. Correspondingly, a large number of intermittency theories have been proposed that specify the form of ζ_p (see discussions by *Frisch* [1995], *Boratav* [1997a], *Schertzer et al.* [1997], and *Sreenivasan and Antonia* [1997]).

Besides the additional information that one obtains from calculating structure functions rather than the variance spectrum, there is also a practical reason for preferring the former over the latter when analyzing observational data: Spectral methods have difficulty dealing with data gaps and uneven sampling, and great care must be taken to avoid spectral leakage, especially with "red noise" type of data [e.g., *Dewan and Grossbard*, 2000]. Structure functions do not have such problems and are easily computed.

For scalars passively advected by turbulence a relation analogous to (4) was established [*Yaglom*, 1949]:

$$\left\langle \delta u_L\,(\delta\theta)^2 \right\rangle = -\frac{4}{3}\epsilon_\theta r\,, \tag{6}$$

where θ is the scalar quantity and ϵ_θ is the mean dissipation rate of its variance. Experimental support for (6) is fairly good [e.g., *Chambers and Antonia*, 1984; *Mydlarski and Warhaft*, 1998]. Intermittency models predicting the form of ζ_p for scalar turbulence are not as well validated [see, e.g., *Frisch et al.*, 1999], but it is clear that anomalous scaling prevails as with the velocity field.

3. Experiment Description

PEM-Tropics B was conducted during March–April 1999. There were 19 flights during the campaign. The TAMMS was operational only during flights 5 to 19, and, unfortunately, the temperature measurements were working properly only from flight 12 onward. All of the relevant flights were over the Pacific (mostly in the central tropical region), except for flight 19, which was a cross-country flight across the United States. The sea surface temperature (SST) in the tropical Pacific were relatively cold due to La Niña conditions, and the region of deep convection was located west of its typical position, with accompanying stronger than normal easterly trade winds. The South Pacific convergence zone was displaced to the west of its normal position, and the intertropical convergence zone was more diffuse and tended to form a double-wall structure [*Hu et al.*, this issue]. A detailed summary of the meteorological conditions are given by *Fuelberg et al.* [this issue]. The routes and brief decriptions for each flight are given in the overview paper [*Raper et al.*, this issue]. A detailed description of the TAMMS is given by *Considine et al.* [1999], and calibration procedures are outlined in *Barrick et al.* [1996]. For this experiment all parameters had a final sampling rate of 22 Hz.

Typically, each flight was composed of several straight and level tracks at different altitudes connected by steep climbs and descents that were either straight or spiraling. As the marine boundary layer was a region of interest, there were a substantial number of flight segments at low altitudes. The P-3B had a flight ceiling of 8 km. Since TAMMS worked best during straight and level flight segments, and because they make the

Table 1. Measured Mean Parameters[a]

Segment	Start, UT	Length, min	z, m	z_i, m	z/z_i	U, m s^{-1}	T, °C	SST, °C	q, g kg^{-1}
1	March 26 2302	26	240	560	0.43	5.2	24	28	16
2	March 31 2010	26	310	630	0.49	4.2	26	29	15
3	March 31 2204	16	300	600	0.50	8.2	26	29	15
4	April 4 2310	12	250	490	0.51	7.5	25	28	14
5	April 4 2325	11	250	490	0.51	8.7	25	28	14
6	April 9 2205	31	290	490	0.59	9.5	24	27	16
7	April 9 2305	11	280	580	0.48	10.9	24	27	15

[a]Local time in Tahiti is UT − 10 hours. U is the mean wind speed.

calculation of structure functions straightforward, we restricted our data analysis to those segments. We defined straight and level as a flight segment that remained within ±30 m in height and ±7.5° in azimuthal heading. In general, the cruising air speeds increased with height, from ~ 130 m s^{-1} in the boundary layer to ~ 160 m s^{-1} in the midtroposphere. The time series data from each straight and level segment were examined carefully for evidence of obvious glitches. Only 18 segments were deemed to have good data for both velocity and temperature.

To reduce statistical noise in the results, one should average as many data values as possible. On the other hand, averages formed from data sets that were obtained under very different conditions make the interpretation and comparison to theory difficult. In data analysis one is often faced with this dilemma. In this study, we chose to examine a limited set of flight segments, which had similar background conditions. Out of the 18 good segments, we narrowed the list to 7 segments that had consistent background states. All of these flights had take-offs and/or landings at Papeete, Tahiti. The list of these segments and their measured mean parameters are given in Table 1, and the corresponding map is shown in Figure 1. The SST was measured by an onboard pyrometer, and the height above surface was measured by radar. Note the similarity in the altitude z, the temperature T, and specific humidity q. The boundary layer height z_i was determined from vertical profiles measured by the aircraft as it descended to or ascended from the flight segments used. We determined that all the segments were in the convectively unstable mixed layer and that the dimensionless height variable z/z_i was in the midsection of the boundary layer for all segments. All of these flight segments were fairly close to local noon, and none of them entered any clouds (D. Morse, Aircraft videotape comments and cloud descriptions in PEM-Tropics B, P-3B, Data Memo 22A, Massachusetts Institute of Technology, April 20, 2000). The lack of clouds, fog, and precipitation circumvents the possible problems in differential pressure probe velocity fluctuation measurements noted by *Paluch and Lenschow* [1991].

4. Results

For each flight segment we used Taylor's hypothesis with the mean air speed to convert the time series into spatial samples. We selected the values $r = (130/22)2^n$ m for integer $n = 0$ to 13 at which to take

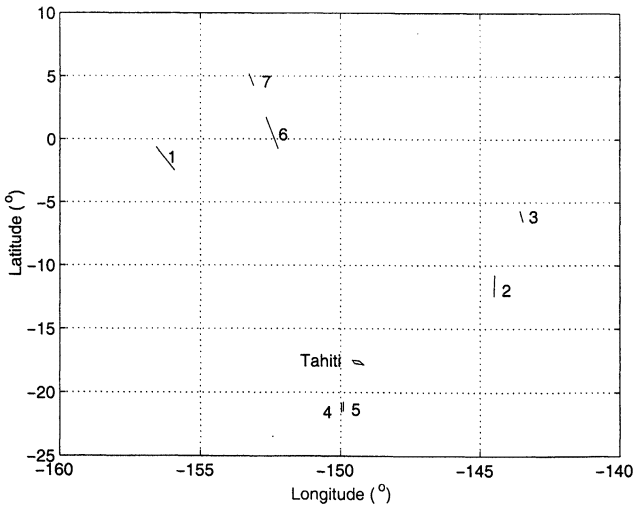

Figure 1. Map of flight segments listed in Table 1.

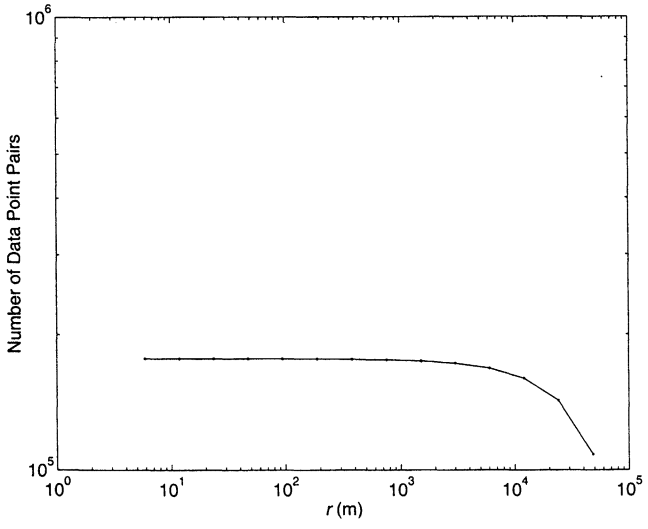

Figure 2. Number of data point pairs used in the calculation of structure functions.

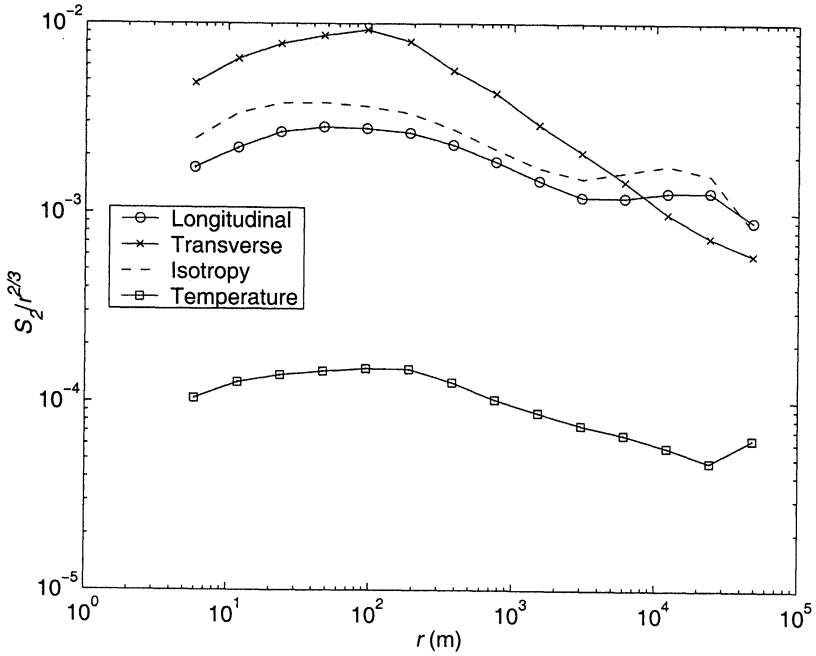

Figure 3. Second-order structure functions divided by $r^{2/3}$. The units are $m^{4/3}\ s^{-2}$ for the velocity functions (top curves) and $K^2\ m^{-2/3}$ for the temperature function (bottom curve).

the differences used in the structure function calculations. For every data point a forward search was conducted for the points that matched closest the specified r values. This scheme yielded even spacing of the results on a logarithmic axis for r. Figure 2 shows the number of data point pairs used in the calculation of the velocity and temperature structure functions.

The second-order structure functions normalized by $r^{2/3}$ are plotted in Figure 3. Normalization by the expected power law allows easy inspection of the data, since then the graphs ought to be straight horizontal lines. The longitudinal and transverse velocity functions are plotted at the top, while the temperature function is at the bottom. The transverse velocity function is calculated as $\langle(\delta u_T)^2\rangle = [\langle(\delta u_{TH})^2\rangle + \langle(\delta u_{TV})^2\rangle]/2$, where u_{TH} is the transverse velocity on the horizontal plane and u_{TV} is the vertical velocity. The dashed line is the second-order structure function for transverse velocity computed using the observed longitudinal second-order function and the isotropy relation [*Monin and Yaglom*, 1975],

$$\left\langle(\delta u_T)^2\right\rangle = \left\langle(\delta u_L)^2\right\rangle + \frac{r}{2}\frac{\partial}{\partial r}\left\langle(\delta u_L)^2\right\rangle . \qquad (7)$$

Variability bars, defined as plus/minus twice the standard deviation divided by the square-root of the number of averages, are also plotted, but they are so small as to be barely visible in Figure 3.

We note that $\langle(u_L)^2\rangle$ shows approximate agreement with the predicted $r^{2/3}$ power law for inertial-range turbulence for r between ~20 and ~200 m. The agreement of $\langle(u_T)^2\rangle$ with isotropy is not good. The drop-off of the transverse component with r is mostly due to the suppression of vertical velocity variance relative to horizontal velocity variance at larger scales, which is expected from stratification for r approaching z_i and beyond. Note that the temperature second-order structure function is similar in form to the velocity functions, with somewhat better agreement with the $r^{2/3}$ power law predicted for scalar advection by inertial-range turbulence [*Obukhov*, 1949; *Corrsin*, 1951].

The normalized velocity third-order structure functions are plotted in Figure 4. The longitudinal third-order function is linear in r up to ~100 m within error bounds, and the sign is negative. This means that the cascade of energy is downscale and (3) may be used to obtain an estimate of the mean energy dissipation rate. From the plot we see that $\epsilon \sim 4 \times 10^{-5}\ m^2\ s^{-3}$. The results for the sum of the longitudinal and two transverse third-order functions are also plotted and shows good agreement with the longitudinal third-order function. Curiously, the sign of the third-order functions change from negative to positive above $r \sim 10$ km. This may be an indication of the presence of an upscale cascade of energy [*Lindborg*, 1999], which is a characteristic of energy-inertial-range two-dimensional (2-D) turbulence [*Kraichnan*, 1967]. This is a possibility for $r > z_i$, because of the strong capping action at the top of the boundary layer. Using the 2-D relation [*Lindborg*, 1999],

$$\left\langle(\delta u_L)^3\right\rangle + \left\langle\delta u_L\,(\delta u_{TH})^2\right\rangle = -2\Pi_u r , \qquad (8)$$

where Π_u is energy flux, we obtain $\Pi_u \sim -10^{-5}\ m^2\ s^{-3}$ for the upscale energy flux. *Högström et al.* [1999] had previously found evidence for 2-D stratified turbulence

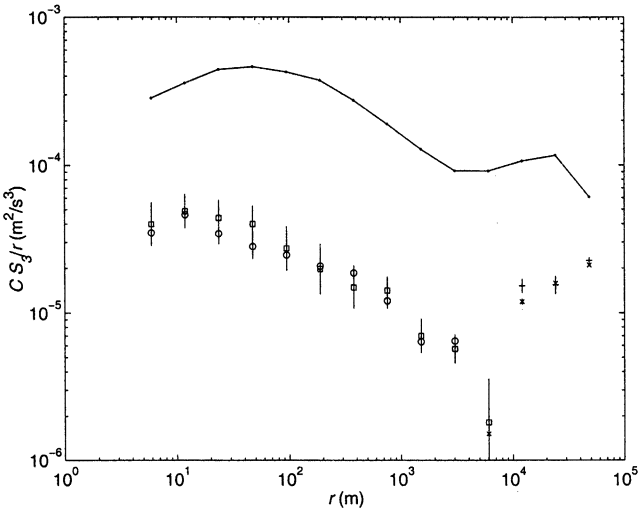

Figure 4. The following third-order structure functions for velocity are multiplied by C and divided by r: The solid line is $\langle|\delta u_L|^3\rangle$, the squares denote $-\langle(\delta u_L)^3\rangle$, the pluses denote $\langle(\delta u_L)^3\rangle$, the circles denote $-\langle(\delta u_L)^3\rangle-\langle(\delta u_{TH})^3\rangle-\langle(\delta u_{TV})^3\rangle$, and the crosses denote $\langle(\delta u_L)^3\rangle+\langle(\delta u_{TH})^3\rangle+\langle(\delta u_{TV})^3\rangle$. The normalization constant C is 5/4 for the curves that involve only longitudinal terms, and 3/4 for the curves that include the transverse terms. Error bars are plus/minus twice the standard deviation divided by the square root of the number of averages.

in the lowest 1 km over an ocean using mostly spectral techniques. However, we believe this is the first instance in which a direct estimate of an upscale energy flux has been made using (8).

For intermittency studies using higher moments we defined the structure functions using absolute values [e.g., *Davis et al.*, 1994]. As one can see from Figure 4, using the absolute value reduces the resultant variability for odd moments, since the distribution of the data increments extend only in the positive direction. Of course, the mean value also increases for odd moments, so the absolute-value moments should not be used to estimate quantities in relations such as (3).

We can also make a comparison with (6). Figure 5 shows $\langle\delta u_L(\delta T)^2\rangle$, where T is temperature, normalized by $4r/3$. The calculated third-order function adheres to a $-r$ law within error bounds up to $r\sim 100$ m. Thus the temperature variance dissipation rate can be estimated to be $\sim 5\times 10^{-7}$ K^2 s^{-1} in the inertial subrange. At the longest scales the sign of $\langle\delta u_L(\delta T)^2\rangle$ reverses as with the velocity third-order structure functions, implying an upscale flow of temperature variance. The 2-D version of (6) is [*Lindborg and Cho*, 2000]

$$\left\langle \delta u_L\,(\delta\theta)^2\right\rangle = -2\Pi_\theta r\,, \tag{9}$$

where Π_θ is the scalar variance flux. From this expression we estimate the upscale temperature variance flux to be $\sim 2\times 10^{-7}$ K^2 s^{-1}.

Now we wish to explore intermittency issues using the higher-order moments of the structure functions. The object is to determine the function ζ_p in (5). The simplest method is to fit straight lines to the structure functions plotted on a log-log scale (the "direct method"). However, it has been noted that variability in the structure functions and deviations away from power law behavior tend to propagate themselves for different order p. Therefore a technique known as extended self-similarity (ESS) has been developed to take advantage of this correlation in variability across the moments [*Benzi et al.*, 1993a]. (Actually, ESS was originally developed to study intermittency in the dissipation subrange, at scales smaller than the break in the inertial-range power law scaling.) The basic idea is to determine the relative scaling between the pth-order and third-order structure functions by plotting them against each other on a log-log plot. From theory, ζ_p is assumed to be 1 for $p=3$, and the other ζ_p values are found from linear fits to the log-log plots. A modified version of this method called generalized extended self-similarity (GESS) [*Benzi et al.*, 1995] uses the normalized functions

$$G_p = \frac{\langle|\delta u|^p\rangle}{\left\langle|\delta u|^3\right\rangle^{\frac{p}{3}}}\,, \tag{10}$$

and relates two different orders of G through $G_p = G_q^{\rho(p,q)}$, where

$$\rho(p,q) = \frac{3\zeta_p - p\zeta_3}{3\zeta_q - q\zeta_3}\,. \tag{11}$$

After ζ_1 is found using ESS, all successive orders of ζ_p can be found by plotting G_p against G_{p-1} and using (11), except for ζ_4, which is obtained from G_4 and

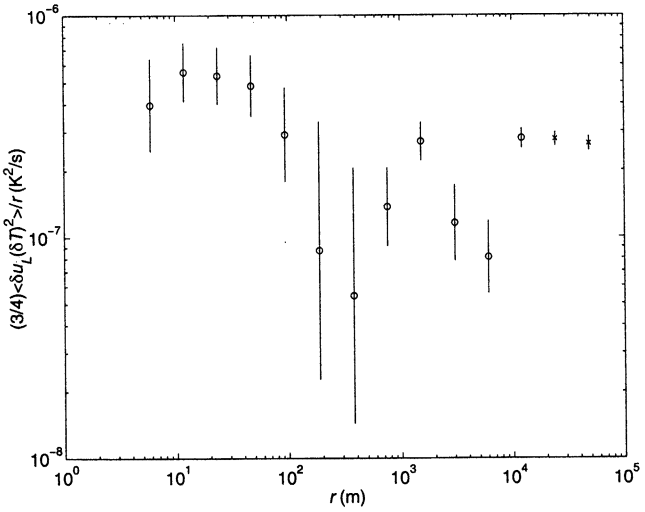

Figure 5. Plot of $\langle\delta u_L(\delta T)^2\rangle$ divided by $4r/3$. Circles denote negative sign and crosses denote positive sign. Error bars are plus/minus twice the standard deviation divided by the square root of the number of averages.

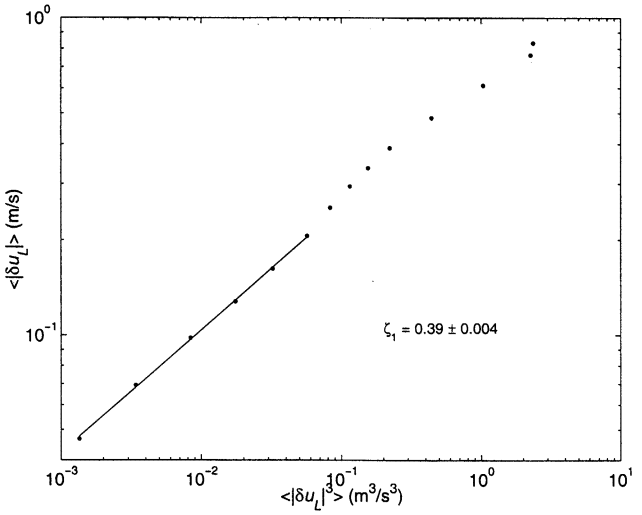

Figure 6. Plot of $\langle|\delta u_L|\rangle$ versus $\langle|\delta u_L|^3\rangle$. The straight line is fitted over the interval r = 6–190 m. Standard error bars in both vertical and horizontal directions are plotted but are too small to be visible.

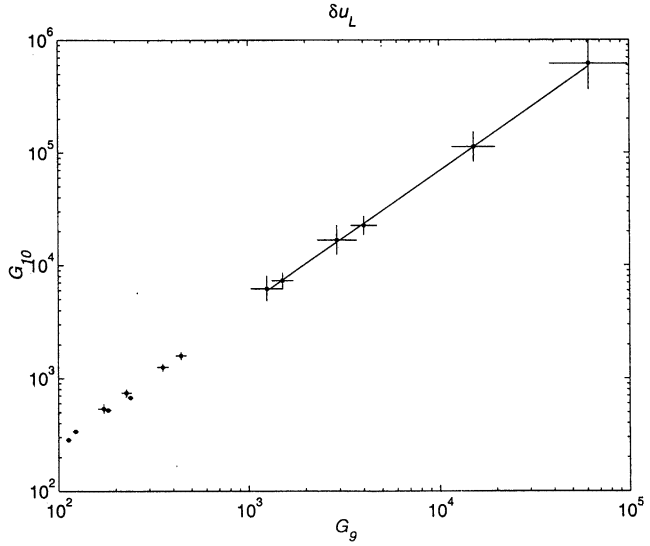

Figure 7. Plot of G_{10} versus G_9 for δu_L. The straight line is fitted over the interval r = 6–190 m.

G_2. Comparisons of the direct method with ESS and GESS have shown that they give quite similar results but that ESS and GESS give progressively less scatter in the computations [*Boratav and Pelz*, 1997]. Our own studies confirm this result. Thus we have chosen to implement GESS in our calculations.

Since ζ_3 must be close to unity for us to have confidence in the validity of the subsequent results, we choose the interval r = 6–190 m (the first six r values; see Figure 4) for the scaling analysis. To show how good the scaling is over this interval, we plot $\langle|\delta u_L|\rangle$ versus $\langle|\delta u_L|^3\rangle$ in Figure 6. This plot represents the first step of using ESS to calculate ζ_1. To show that the scaling holds even at high orders, we plot G_{10} versus G_9 in Figure 7. The scalings for δu_T and δT were likewise very good, although the uncertainties in the fits were considerably greater for δu_T.

The resultant ζ_p values for δu_L and δu_T are shown in Figures 8 and 9. Along with the scaling calculated from the entire data set (circles), we also calculated the mean of the scaling parameters calculated for 2755 64-point segments (squares). The former corresponds to parameters that are computed from the ensemble average of many realizations, while the latter corresponds to

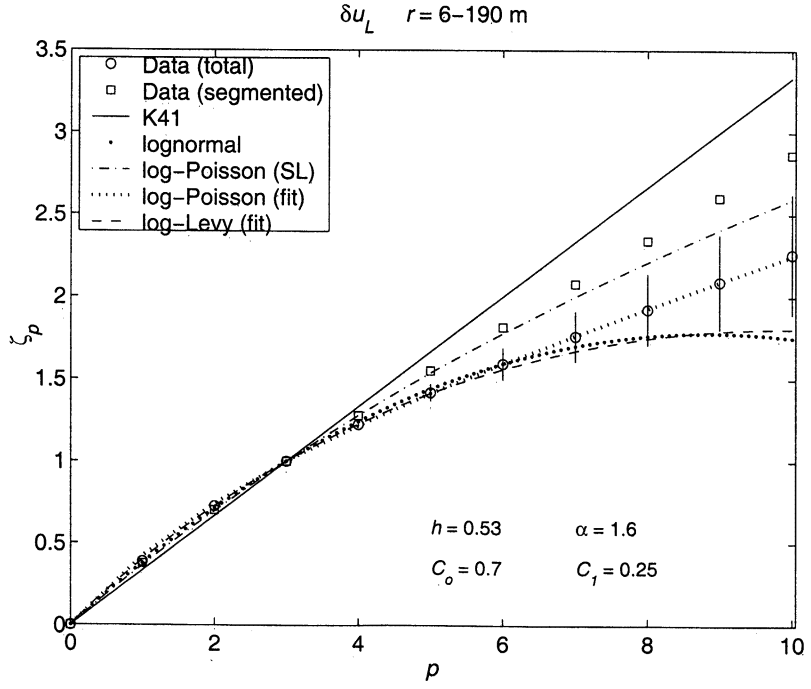

Figure 8. Plot of ζ_p versus p for δu_L.

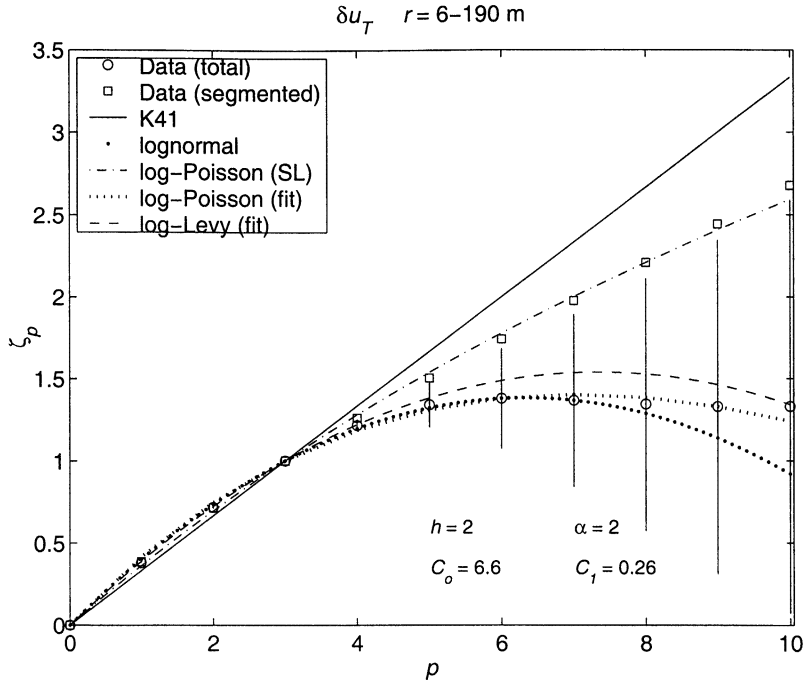

Figure 9. Plot of ζ_p versus p for δu_T.

the mean of parameters computed from ~1 realization (we say "many" and "~1" because the physical length of an N-point segment varied with the aircraft speed). For brevity, let us label the former case "total" and the latter case "segmented." Note that error bars are plotted for both cases, but they are too small to be visible in the latter. Later, we will discuss the implications of the difference between the two results.

We have also plotted four of the best known models: the K41 (mentioned earlier), the lognormal [*Kolmogorov*, 1962; *Obukhov*, 1962], the log-Poisson [*She and Leveque*, 1994], and the log-Lévy [*Schertzer and Lovejoy*, 1987] models. Any required input values were taken from the total data results. The scalings are clearly anomalous for both the total and segmented results, and indicate more intermittency than predicted by the K41 theory.

The lognormal model has been criticized because it violates Novikov's inequality [*Novikov*, 1970] and the nondecreasing criterion of *Frisch* [1991], although these two conditions themselves have been questioned on their relevance to real fluids [*Schertzer et al.*, 1995]. The log-Poisson model has had success in matching experimental data [e.g., *Anselmet et al.*, 1984; *Benzi et al.*, 1993b], but it has also been criticized as implying a nonphysical probability distribution function [*Novikov*, 1994]. More recently, *Boratav and Pelz* [1997] have provided evidence from numerical simulations that the transverse velocity intermittency is greater than the longitudinal velocity intermittency, and that the former is also more intermittent than predicted by the original She-Lévêque log-Poisson model (labeled in Figures 8 and 9 as "log-Poisson (SL)"). They were able to fit their data more closely for both cases by freeing two parameters in a generalized form of the log-Poisson model. Our results provide experimental support for this disparity in intermittency between the longitudinal and transverse velocity fields, especially for the segmented data case, where the statistical uncertainties are very small.

The log-Poisson model can also be expressed as a function of the time scale exponent h and codimension C_o of the most intermittent structures [*Politano and Pouquet*, 1995]:

$$\zeta_p = (1-h)\frac{p}{3} + C_o\left[1 - \left(1 - \frac{h}{C_o}\right)^{\frac{p}{3}}\right] . \qquad (12)$$

She and Leveque [1994] chose $h = 2/3$ and $C_o = 2$. Other choices, however, can be justified [e.g., *Chen and Cao*, 1995]. Equation (12) can also be fit to the data by determining these two parameters from the measured ζ_6 and ζ_9: $h = (2-\zeta_6)^2/(3-3\zeta_6+\zeta_9)$ and $C_o = (2-\zeta_6)^3/(3-3\zeta_6+\zeta_9)^2$. The resulting values and the consequent plots of (12) are displayed in Figures 8 and 9.

The log-Lévy model for velocity yields similar predictions to the log-Poisson model, but *Schertzer et al.* [1995] advocates its use because of its "strong universality" properties. One of the key differences between the two models is that the log-Poisson predicts ζ_p to be independent of the number of realizations. This is clearly not true for our results (Figures 8 and 9). The log-Lévy model on the other hand allows for a divergence in moments at a critical value, p_c, which leads to a change in ζ_p for $p \geq p_c$ with the number of realizations considered. More specifically, ζ_p reaches a linear asymptote

Table 2. Calculated Parameters for ζ_p Asymptotes

Type	Segmented		Total	
	γ	C_I	γ	C_I
δu_L	-0.27 ± 0.001	0.19 ± 0.002	-0.17 ± 0.04	0.57 ± 0.23
δu_T	-0.24 ± 0.001	0.27 ± 0.002	...	...
δT	-0.22 ± 0.003	0.32 ± 0.02	-0.13 ± 0.02	0.73 ± 0.11

for $p \geq p_c$, expressed as $\zeta_p = C_I - \gamma p$. (See *Schertzer et al.* [1997] for a more detailed discussion.) For both δu_L and δu_T we observe such an asymptotic behavior. The transition can be either first or second order, with the critical moment of the former being independent of the number of realizations, while the critical moment of the latter being sampling dependent. It appears from Figures 8 and 9 that p_c does depend on the number of realizations. For the segmented data the linear asymptote reaches down to $p \sim 3$, while for the total data the asymptote only goes down to $p \sim 5$. For confirmation we calculate the second-order transition moment, $p_s = 3(C_I/C_1)^{1/\alpha}$ [*Schmitt et al.*, 1994]. For δu_L we obtain $p_s = 2.6$ and 5.0 for the segmented and total data cases. For δu_T segmented, we obtain $p_s = 3.2$ (the total data case had error bars too large for a meaningful result). These values are consistent with the observed transition moments, so we seem to have second-order transitions here. Values of C_I and γ derived from linear fits to the data for $p \geq p_c$ are given in Table 2. Values for the δu_T total data case are not given, because the uncertainties were larger than the values themselves.

The scaling exponents ζ_p for the log-Lévy model are given by

$$\zeta_p = \frac{p}{3} - \frac{C_1}{\alpha - 1}\left[\left(\frac{p}{3}\right)^{\alpha} - \frac{p}{3}\right] , \qquad (13)$$

where C_1 is the mean fractality parameter (or codimension of the mean singularity) and α, the Lévy index, can be varied to fit the data. The mean fractality parameter can be calculated from the data through $C_1 = 1 - 3(d\zeta_p/dp)|_{p=3}$. The resulting values and the subsequent plots of (13) are shown in Figures 8 and 9. Following the logic of the multifractal phase transition [*Schertzer and Lovejoy*, 1992], the fits were performed only up to $p = p_c = 5$ (to the total data), beyond which the fit to the empirical results is not expected to be good. For the longitudinal velocity results the values of $\alpha = 1.6$ and $C_1 = 0.25$ compare favorably to past atmospheric measurements of $\alpha = 1.45 \pm 0.1$ and $C_1 = 0.24 \pm 0.05$ [*Schmitt et al.*, 1993], although other experiments have yielded somewhat smaller values of C_1 [e.g., *Schertzer et al.*, 1995]. These values are also very close to those calculated from numerical simulations of the scaling gyroscope cascade model [*Schertzer et al.*, 1997].

Although ESS has been applied to passive scalar data [e.g., *Benzi et al.*, 1994; *Ruiz Chavarria et al.*, 1995], unlike for the case of velocity structure functions, there is no theoretical basis for assigning a reference value like $\zeta_3 = 1$. It is possible to use a measured reference instead, but we elected to use the direct method for computing the slopes of the temperature structure functions, since it yielded more consistent results for different numbers of realizations. We chose the interval $r = 12$–190 m, since the instrument response time of the temperature probe at the full 22 Hz (~6-m interval) was somewhat suspect. The results are shown in Figure 10.

To derive theoretical models for the scaling of temperature structure functions, some assumption needs to be made for the correlation between Π_u and Π_θ, the energy flux and scalar variance flux. Although it seems reasonable to posit only a partial correlation between the two quantities, for our temperature data the best fit to proposed models occurred when a complete correlation was assumed, i.e., that ζ_p is the same for both velocity and temperature data. In Figure 10 the model curves from Figure 8 are reproduced, except for the She-Lévêque model. In addition, the predictions for a random advection/diffusion model with a white Gaussian velocity field δ-correlated in time with self-similar correlations in a spatial dimension of three [*Kraichnan*, 1994] is also plotted. We tried fitting bivariate models that allowed for partial correlation between Π_u and Π_θ [*Van Atta*, 1971, 1973; *Schmitt et al.*, 1996; *Cao and Chen*, 1997], but these could not fit our data very well. We note, however, that our ζ_p curve for temperature data was significantly less multifractal than previous results [e.g., *Antonia et al.*, 1984; *Ruiz Chavarria et al.*, 1995].

As before, we have also calculated the ζ_ps for the mean of order-unity realizations (labeled segmented). Again we see a divergence of moments for the different numbers of realizations, with the ζ_ps going to a linear asymptote at high values. Although difficult to see from the plot, the linear asymptote for the segmented data results goes down to $p \sim 4$, while for the total data it extends down to $p \sim 6$. Thus the multifractal phase transition appears to be of second order. To check for consistency, we calculated p_s as we did for the velocity parameters, and obtained the values 3.5 and 5.9 for the segmented and total data cases. The parameters derived from the linear asymptotic fits are given in Table 2. As for the velocity results, the intercept C_I increases and the slope $-\gamma$ decreases with the number of realizations.

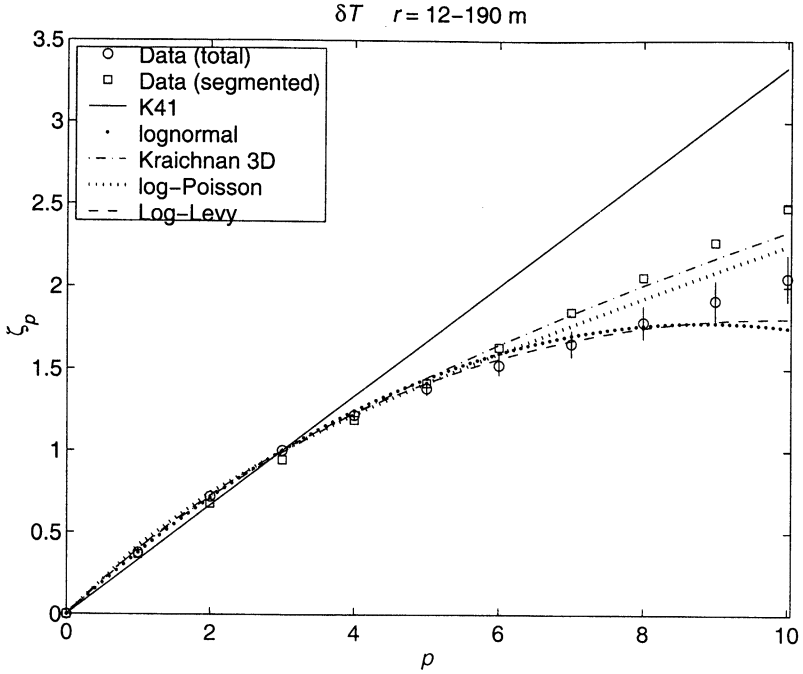

Figure 10. Plot of ζ_p versus p for δT.

5. Summary Discussion

Using aircraft data collected for an experiment not specifically designed for turbulence studies brings up the issues of ergodicity and homogeneity. Ideally, one should either have so much data that one can reasonably talk about the mean state of the atmosphere, or one should examine data collected under strictly specified conditions. Since our study lies somewhere in between these two extreme cases, one must be wary in interpreting the results. The higher-order calculations (where anomalies are emphasized) are especially susceptible to slight changes in conditions. Our scaling results seem to show second-order multifractal phase transitions implying that, indeed, sampling was an issue. Therefore the actual numerical values derived from our computations should be taken with a grain of salt. We can say something, however, about the qualitative behavior of the structure functions and what the real atmosphere is like relative to the idealized theories.

The appearance of multifractal phase transitions in both velocity and temperature data, and the change in asymptote with the number of realizations, was a key result. As pointed out by *Schertzer et al.* [1995], these characteristics argue against the log-Poisson model. For our velocity data, then, the log-Lévy model becomes the better alternative, begin able to fit the ζ_p curves up to the transition point, and also able to accommodate the asymptotic change.

Another interesting result was the difference in intermittency between the longitudinal and transverse velocity fields, with the latter being more multifractal than the former, both for small and large numbers of realizations. (For the latter case, however, the large error bars in the transverse velocity results precluded a precise estimate of the difference.) Such differences were noted recently in direct numerical simulations [*Boratav and Pelz*, 1997]. This qualitative result remained constant when different subsets of the data were used, and it held for the case where only the horizontal transverse velocity was used, i.e., when the vertical velocity, always the most problematic to measure, was excluded. The difference therefore does seem to be a real characteristic. The reason for the difference in intermittency between the longitudinal and transverse velocity components may very well be the anisotropy observed in Figure 3. Although the numerical simulation used to study this issue conformed fairly well to isotropy, the question of whether the difference in intermittency is caused by slight anisotropies or is characteristic of isotropic turbulence remains an open question [*Boratav*, 1997b].

The temperature results did not show signs of saturation as have been postulated [*Chertkov*, 1997; *Balkovsky and Lebedev*, 1998] up to order 10. *Frisch et al.* [1999] have argued that saturation has general validity, even though the orders where it can be observed may be too high depending on the spatial dimension and the roughness of the velocity field. However, as noted above, the results did indicate a second-order multifractal phase transition, and, curiously, the scaling parameters were very similar to the velocity results up to the transition moment. Again, the divergence of moments for different numbers of realizations is evidence against the log-Poisson model.

We were also able to estimate the strength and direction of the kinetic energy and temperature variance cascades. The cascades for both quantities were downscale in the presumed inertial subrange, with dissipation

rates of $\epsilon \sim 4 \times 10^{-5}$ m^2 s^{-3} and $\epsilon_\theta \sim 5 \times 10^{-7}$ K^2 s^{-1}. For $r > 10$ km the energy appeared to flow in a 2-D upscale cascade with a flux of $\sim 10^{-5}$ m^2 s^{-3}. Beginning at somewhat longer scales, the temperature variance also had a 2-D upscale flux of $\sim 2 \times 10^{-7}$ K^2 s^{-1}.

Acknowledgments. The MIT work was funded by NASA grant NAG1-2173. We wish to thank Donald Bagwell for putting together the TAMMS data acquisition system and providing programming support. JYNC would like to thank Erik Lindborg for helpful discussions on related topics.

References

Anselmet, F., Y. Gagne, E. J. Hopfinger, and A. Antonia, High-order velocity structure functions in turbulent shear flows, *J. Fluid Mech.*, *140*, 63–89, 1984.

Antonia, R. A., E. J. Hopfinger, Y. Gagne, and F. Anselmet, Temperature structure functions in turbulent shear flows, *Phys. Rev. A*, *30*, 2704–2707, 1984.

Antonia, R. A., M. Ould-Rouis, F. Anselmet, and Y. Zhu, Analogy between predictions of Kolmogorov and Yaglom, *J. Fluid Mech.*, *332*, 395–409, 1997.

Balkovsky, E., and V. Lebedev, Instanton for the Kraichnan random advection model, *Phys. Rev. E Stat. Phys. Plasmas Fluids Relat. Interdiscip. Top.*, *58*, 5776–5795, 1998.

Barrick, J. D. W., J. A. Ritter, C. E. Watson, M. W. Wynkoop, J. K. Quinn, and D. R. Norfolk, Calibration of NASA turbulent air motion measurement system, *NASA Tech. Pap. TP-3610*, 1996.

Benzi, R., S. Ciliberto, C. Baudet, G. R. Chavarria, and R. Tripiccione, Extended self-similarity in the dissipation range of fully developed turbulence, *Europhys. Lett.*, *24*, 275–279, 1993a.

Benzi, R., S. Ciliberto, R. Tripiccione, C. Baudet, F. Massaioli, and S. Succi, Extended self-similarity in turbulent flows, *Phys. Rev. E*, *48*, R29–R32, 1993b.

Benzi, R., F. Massaioli, S. Succi, and R. Tripiccione, Scaling behavior of the velocity and temperature correlation functions in 3D convective turbulence, *Europhys. Lett.*, *28*, 231–236, 1994.

Benzi, R., L. Biferale, S. Ciliberto, M. V. Struglia, and R. Tripiccione, On the intermittent energy transfer at viscous scales in turbulent flows, *Europhys. Lett.*, *32*, 709–713, 1995.

Boratav, O., On recent intermittency models of turbulence, *Phys. Fluids*, *9*, 1206–1208, 1997a.

Boratav, O., On longitudinal and lateral moment hierarchy in turbulence, *Phys. Fluids*, *9*, 3120–3122, 1997b.

Boratav, O., and R. B. Pelz, Structures and structure functions in the inertial range of turbulence, *Phys. Fluids*, *9*, 1400–1415, 1997.

Cao, N., and S. Chen, An intermittency model for passive-scalar turbulence, *Phys. Fluids*, *9*, 1203–1205, 1997.

Chambers, A. J., and R. A. Antonia, Atmospheric estimates of power law exponents μ and μ_θ, *Boundary Layer Meteorol.*, *28*, 343–352, 1984.

Chen, S., and N. Cao, Inertial range scaling in turbulence, *Phys. Rev. E*, *52*, R5757–R5759, 1995.

Chertkov, M., Instanton for random advection, *Phys. Rev. E Stat. Phys. Plasmas Fluids Relat. Interdiscip. Top.*, *55*, 2722–2735, 1997.

Cho, J. Y. N., and E. Lindborg, Horizontal velocity structure functions in the upper troposphere and lower stratosphere, 1, Observations, *J. Geophys. Res.*, *106*, 10,223–10,232, 2001.

Cho, J. Y. N., R. E. Newell, and G. W. Sachse, Anomalous scaling of mesoscale tropospheric humidity fluctuations, *Geophys. Res. Lett.*, *27*, 377–380, 2000.

Cho, J. Y. N., V. Thouret, R. E. Newell, and A. Marenco, Isentropic scaling analysis of ozone in the upper troposphere and lower stratosphere, *J. Geophys. Res.*, *106*, 10,023–10,038, 2001.

Considine, G. D., B. Anderson, J. Barrick, and D. H. Lenschow, Characterization of turbulent transport in the marine boundary layer during flight 7 of PEM-Tropics A, *J. Geophys. Res.*, *104*, 5855–5863, 1999.

Corrsin, S., On the spectrum of isotropic temperature fluctuations in an isotropic turbulence, *J. Appl. Phys.*, *22*, 469–473, 1951.

Davis, A., A. Marshak, W. Wiscombe, and R. Cahalan, Multifractal characterizations of nonstationarity and intermittency in geophysical fields: Observed, retrieved, or simulated, *J. Geophys. Res.*, *99*, 8055–8072, 1994.

Dewan, E. M., and N. Grossbard, Power spectral artifacts in published balloon data and implications regarding saturated gravity wave theories, *J. Geophys. Res.*, *105*, 4667–4684, 2000.

Frisch, U., From global scaling à la Kolmogorov, to local multifractal in fully developed turbulence, *Proc. R. Soc. London, Ser. A*, *434*, 89–99, 1991.

Frisch, U., *Turbulence: The Legacy of A. N. Kolmogorov*, 296 pp., Cambridge Univ. Press, New York, 1995.

Frisch, U., A. Mazzino, and M. Vergassola, Lagrangian dynamics and high-order moments intermittency in passive scalar advection, *Phys. Chem. Earth B*, *24*, 945–951, 1999.

Fuelberg, H. E., R. E. Newell, D. J. Westberg, J. C. Maloney, J. R. Hannan, B. C. Martin, M. A. Avery, and Y. Zhu, A meteorological overview of the second Pacific Exploratory Mission in the tropics, *J. Geophys. Res.*, this issue.

Högström, U., A.-S. Smedman, and H. Bergström, A case study of two-dimensional stratified turbulence, *J. Atmos. Sci.*, *56*, 959–976, 1999.

Hu, Y., R. E. Newell, and Y. Zhu, Mean moist circulation for PEM-Tropics missions, *J. Geophys. Res.*, this issue.

Kolmogorov, A. N., The local structure of turbulence in incompressible viscous fluid for very large Reynolds number, *Dokl. Akad. Nauk SSSR*, *30*, 299–303, 1941a.

Kolmogorov, A. N., Dissipation of energy in locally isotropic turbulence, *Dokl. Akad. Nauk SSSR*, *32*, 16–18, 1941b.

Kolmogorov, A. N., The equation of turbulent motion in an incompressible viscous fluid, *Izv. Akad. Nauk SSSR, Ser. Fiz.*, *6*, 56–58, 1942.

Kolmogorov, A. N., A refinement of previous hypotheses concerning the local structure of turbulence in a viscous incompressible fluid at high Reynolds number, *J. Fluid Mech.*, *13*, 82–85, 1962.

Kraichnan, R., Anomalous scaling of a randomly advected passive scalar, *Phys. Rev. Lett.*, *72*, 1016–1019, 1994.

Kraichnan, R. H., Inertial ranges in two-dimensional turbulence, *Phys. Fluids*, *10*, 1417–1423, 1967.

Lindborg, E., A note on Kolmogorov's third-order structure-function law, the local isotropy hypothesis and the pressure-velocity correlation, *J. Fluid Mech.*, *326*, 343–356, 1996.

Lindborg, E., Can the atmospheric kinetic energy spectrum be explained by two-dimensional turbulence?, *J. Fluid Mech.*, *388*, 259–288, 1999.

Lindborg, E., and J. Y. N. Cho, Determining the cascade of passive scalar variance in the lower stratosphere, *Phys. Rev. Lett.*, *85*, 5663–5666, 2000.

Lindborg, E., and J. Y. N. Cho, Horizontal velocity structure functions in the upper troposphere and lower stratosphere, 2, Theoretical considerations, *J. Geophys. Res.*, *106*, 10,233–10,242, 2001.

Monin, A. S., and A. M. Yaglom, *Statistical Fluid Mechanics: Mechanics of Turbulence*, vol. 2, 874 pp., MIT Press, Cambridge, Mass., 1975.

Mydlarski, L., and Z. Warhaft, Passive scalar statistics in high-Péclet-number grid turbulence, *J. Fluid Mech.*, *358*, 135–175, 1998.

Novikov, E. A., Intermittency and scale similarity of the structure of turbulent flow, *Prikl. Math. Mekh.*, *35*, 266–277, 1970.

Novikov, E. A., Infinitely divisible distributions in turbulence, *Phys. Rev. E*, *50*, R3303–R3305, 1994.

Obukhov, A. M., Structure of the temperature field in turbulent flow, *Izv. Akad. Nauk SSSR, Ser. Geogr. Geofiz.*, *13*, 58–69, 1949.

Obukhov, A. M., Some specific features of atmospheric turbulence, *J. Fluid Mech.*, *13*, 77–81, 1962.

Paluch, I. R., and D. H. Lenschow, Stratiform cloud formation in the marine boundary layer, *J. Atmos. Sci.*, *48*, 2141–2158, 1991.

Politano, H., and A. Pouquet, Model of intermittency in magnetohydrodynamic turbulence, *Phys. Rev. E*, *52*, 636–641, 1995.

Raper, J. L., M. M. Kleb, D. J. Jacob, D. D. Davis, R. E. Newell, H. E. Fuelberg, R. J. Bendura, J. M. Hoell, and R. J. McNeal, Pacific Exploratory Mission in the tropical Pacific: PEM-Tropics B, March-April 1999, *J. Geophys. Res.*, this issue.

Ruiz Chavarria, G., C. Baudet, and S. Ciliberto, Extended self-similarity of passive scalars in fully developed turbulence, *Europhys. Lett.*, *32*, 319–324, 1995.

Schertzer, D., and S. Lovejoy, Physical modeling and analysis of rain and clouds by anisotropic scaling multiplicative processes, *J. Geophys. Res.*, *92*, 9693–9714, 1987.

Schertzer, D., and S. Lovejoy, Hard and soft multifractal processes, *Phys. A*, *185*, 187–194, 1992.

Schertzer, D., S. Lovejoy, and F. Schmitt, Stuctures in turbulence and multifractal universality, in *Small-Scale Structures in Three-Dimensional Hydrodynamic and Magnetohydrodynamic Turbulence,* edited by M. Meneguzzi, A. Pouquet, and P.-L. Sulem, pp. 137–144, Springer-Verlag, New York, 1995.

Schertzer, D., S. Lovejoy, F. Schmitt, Y. Chigirinskaya, and D. Marsan, Multifractal cascade dynamics and turbulent intermittency, *Fractals*, *5*, 427–471, 1997.

Schmitt, F., D. Schertzer, S. Lovejoy, and Y. Brunet, Estimation of universal multifractal indices for atmospheric turbulent velocity fields, *Fractals*, *1*, 568–575, 1993.

Schmitt, F., D. Schertzer, S. Lovejoy, and Y. Brunet, Empirical study of multifractal phase transitions in atmospheric turbulence, *Nonlin. Proc. Geophys.*, *1*, 95–104, 1994.

Schmitt, F., D. Schertzer, S. Lovejoy, and Y. Brunet, Multifractal temperature and flux of temperature variance in fully developed turbulence, *Europhys. Lett.*, *34*, 195–200, 1996.

She, Z.-S., and E. Leveque, Universal scaling laws in fully developed turbulence, *Phys. Rev. Lett.*, *72*, 336–339, 1994.

Sreenivasan, K. R., and R. A. Antonia, The phenomenology of small-scale turbulence, *Ann. Rev. Fluid Mech.*, *29*, 435–472, 1997.

Van Atta, C. W., Influence of fluctuations in local dissipation rates on turbulent scalar characteristics in the inertial subrange, *Phys. Fluids*, *14*, 1803–1804, 1971.

Van Atta, C. W., Erratum: Influence of fluctuations in local dissipation rates on turbulent scalar characteristics in the inertial subrange, *Phys. Fluids*, *16*, 574, 1973.

Vincent, A., and M. Meneguzzi, The spatial structure and statistical properties of homogeneous turbulence, *J. Fluid Mech.*, *225*, 1–25, 1991.

von Kármán, T., and L. Howarth, On the statistical theory of isotropic turbulence, *Proc. R. Soc. London, Ser. A*, *164*, 192–215, 1938.

Yaglom, A. M., On the local structure of a temperature field in a turbulent flow, *Dokl. Akad. Nauk SSSR*, *69*, 743–746, 1949.

B. E. Anderson, J. D. W. Barrick, and K. L. Thornhill, Mail Stop 483, NASA Langley Research Center, 21 Langley Boulevard, Hampton, VA 23681-2199. (b.e.anderson@larc.nasa.gov; j.d.barrick@larc.nasa.gov; k.l.thornhill@larc.nasa.gov)

J. Y. N. Cho, Department of Earth, Atmospheric, and Planetary Sciences, Massachusetts Institute of Technology, 77 Massachusetts Avenue, Room 54-1823, Cambridge, MA 02139-4307. (jcho@pemtropics.mit.edu)

(Received August 29, 2000; revised January 23, 2001; accepted January 24, 2001.)